Received: 13 February 2020 | Revised: 12 April 2020 | Accepted: 8 June 2020

DOI: 10.1002/htj.21843

RESEARCH ARTICLE

HEAT TRANSFER WILEY

Energy and mass transport of micropolar nanofluid flow over an inclined surface with Keller-Box simulation

Khuram Rafique[1] | **Muhammad Imran Anwar**[1,2,3] | **Masnita Misiran**[1] | **Muhammad Imran Asjad**[4]

[1]School of Quantitative Sciences, Universiti Utara Malaysia, Sintok, Malaysia

[2]Department of Mathematics, Faculty of Science, University of Sargodha, Sargodha, Pakistan

[3]Higher Education Department, Lahore, Pakistan

[4]Department of Mathematics, University of Management and Technology Lahore, Lahore, Pakistan

Correspondence
Muhammad Imran Asjad, Department of Mathematics, University of Management and Technology Lahore, Lahore 54770, Pakistan.
Email: imran.asjad@umt.edu.pk

Abstract

In this article, micropolar nanofluid boundary layer flow over a slanted stretching surface with Soret and Dufour effect is studied. The inclined stretching surface in this study is considered permeable and linear. In this problem, the Buongiorno model is considered for thermal efficiencies of fluid flow in the existence of Brownian movement and thermophoresis properties. The nonlinear problem for Micropolar Nanofluid flow over the slanted channel is developed to think about the heat and mass exchange phenomenon by incorporating portent flow factors to strengthened boundary layers. In this study, nonlinear partial differential equations are converted to nonlinear ordinary differential equations by utilizing appropriate similarity transformations then elucidated the numerical outcomes by the Keller-Box technique. An examination of the set-up results is performed with accessible outcomes and perceived in a good settlement without involved impacts. Numerical and graphical outcomes are additionally displayed in tables and charts.

KEYWORDS

Dufour, inclined surface, MHD, micropolar nanofluid, permeable, Soret

1 | INTRODUCTION

Dynamics of fluid flows induced by stretchable surface has achieved much consideration. It is because of their broad applications in designing and industrial processes. Especially, the boundary layer flow toward a slanted extending surface has gotten perceptible thought of the ongoing scientists in view of its modern and building utilizes, including material fabricated by expulsion, paper making, hot moving, production of plastic, and versatile expulsion. Sakiadis[1] initiated the investigation on the laminar boundary layer flow on a continuous moving surface. Later, Crane[2] enhanced the discussion on the linearly extending surface. Noor et al[3] explained the thermophoretic flow on a slanted sheet. Tshehla[4] discussed the flow of the fluid on a slanted plate. Besides, non-Newtonian fluid flow through slanted sheet was investigated by Bognár et al.[5] Moreover, Hamza et al[6] examined the flow over an inclined surface by using the finite difference technique. Recently, Raju[7] studied the non-Newtonian fluid flow on an inclined sheet by incorporating the thermal radiations. Non-Newtonian fluid flow over the vertically slanted plate is investigated by Reddy et al.[8] Singh[9] studied the flow of viscous liquid over the slanted sheet.

Nanofluids are a mix of metallic particles that are drenched in regular fluids that have low thermal conductivity. Thermal properties of the base liquid significantly improved, when nanoparticles are included the convectional liquids Das et al[10] and Buongiorno[11] distinguished two slip systems out of seven, which assume key job to improve the thermal conductivity of base fluids are Brownian movement and thermophoresis. Nanoparticles slam into one another in the base liquid because of the Brownian movement. In fact, thermal conductivity improved because of the impacts of nanoparticles. Ultrahigh-execution cooling is a standout among the most fundamental needs of various mechanical developments. However, the low thermal conductivity of conventional fluid put fundamental limitation in emerging energy-efficient heat exchange liquids that are necessary for ultrahigh-performance cooling. Sandeep and Kumar[12] examined the dusty nanofluid flow over an extending slanted sheet. Rashad[13] studied the flow of nanofluid over an inclined sheet. Govindarajan[14] discussed nanofluid flow over an inclined sheet by considering the surface temperature. Suriyakumar and Devi[15] studied the nanofluid flow through inclined sheet by taking suction in account. Khan et al[16] investigated Carreau nanofluid flow on the stretching sheet. Chakraborty et al[17] calculated the heat influence on nanofluid flow on the slanted sheet. A similarity solution of nanofluid flow over slanted surface was discussed by Ziaei-Rad et al.[18] Afify[19] investigated the non-Newtonian fluid flow over inclined sheet by incorporating the chemical reaction. Halim et al[20] studied the Williamson nanofluid flow over stretching and shrinking sheet. In addition, Sher Akbar[21] discussed boundary condition effects on flow of nanofluids. Latest work on energy and mass transport of nanofluid flow over an inclined surface was done by Rafique et al.[22]

Soret and Dufour effects have gotten significant attention of numerous investigators. These effects play key roles in the areas, for example, hydrology, petrology, geosciences, and so forth. Bég et al[23] considered the Newtonian fluid on a slanted sheet. Pal and Chatterjee[24] studied the Soret and Dufour effects on a nonlinear inclined sheet. Balla and Naikoti[25] scrutinized the Soret and Dufour impacts on inclined cavity. Sravanthi[26] studied the homotopy analysis of micropolar fluid on slanted sheet by incorporating the Soret and Dufour effects.

The idea of the micropolar liquid has accomplished incredible significance as the regular Newtonian fluids cannot exactly signify the features of fluid flow in various mechanical uses, in particular, polymeric liquids, science, colloidal arrangements, and paints. Micropolar liquids are physically described liquids in which the twisting of the components excluded in the liquids

and containing a suspension of inflexible, round molecules in a viscid medium. Eringen[27] was the first who introduced the hypothesis about micropolar liquid and covering in both model and applications than the ordinary one. By considering the variable fluid properties the micropolar fluid flow on a slanted sheet discussed by Rahman et al.[28] Uddin[29] investigated the micropolar fluid flow by incorporating the electrical conductivity on the inclined surface. Heat and mass exchange of micropolar liquid stream along a slanted sheet examined by Das[30]. Anwar et al[31] scrutinized the micropolar nanofluid stream on extending sheet by the Keller-Box scheme. Hazbavi and Sharhani[32] analyzed the micropolar fluid flow among two inclined sheets by considering pressure gradient constant. Effect of double dispersion on micropolar fluid flow on inclined sheet studied by Srinivasacharya et al.[33] Srinivasacharya and Bindu[34] discussed the micropolar fluid flow in slanted channel numerically. Shamshuddin et al[35] studied the micropolar fluid flow by considering the Joule heating. Noor et al[36] investigated micropolar nanofluid flow toward a vertical surface. Recently, Rafique et al[37] discussed the energy and mass exchange phenomenon of micropolar nanofluid flow over a slanted surface.

In view of the above-cited literature, no study yet conducted to investigate heat and mass exchange of micropolar type nanofluid flow by incorporating Soret and Dufour effects over a permeable stretching inclined surface. To fill this gap in literature, we are considering the study under concern for numerical simulation via the Keller-Box scheme, which is the novelty of current problem.

2 | PROBLEM FORMULATION

A steady, two-dimensional boundary layer flow of micropolar nanofluid over a linear inclined extending surface by considering an angle γ. The extending and free stream velocities are taken as, $u_w(x) = ax$ and $u_\infty(x) = 0$. Where, x is the coordinate dignified in the direction of extending surface with a suppose constant. An external transverse magnetic field is assumed normal to the flow path. It is supposed that the electric and magnetic field properties are very insignificant as the magnetic Reynolds number is less.[38] The micropolar finite-size particles along with nanoparticles are constantly distributed in the base fluids. The fluid particles have extra space to travel about formerly hitting to the other fluid particle, where these particles revolve in the fluid field and fallouts for spinning effects in the micropolar nanofluid. The Brownian motion and thermophoresis impacts are incorporated. The temperature T and nanoparticle fraction C at the wall take the constant values T_w and C_w, while the ambient forms for nanofluid mass and temperature fractions C_∞ and T_∞ are accomplished as y approaches to immensity shown in Figure 1.

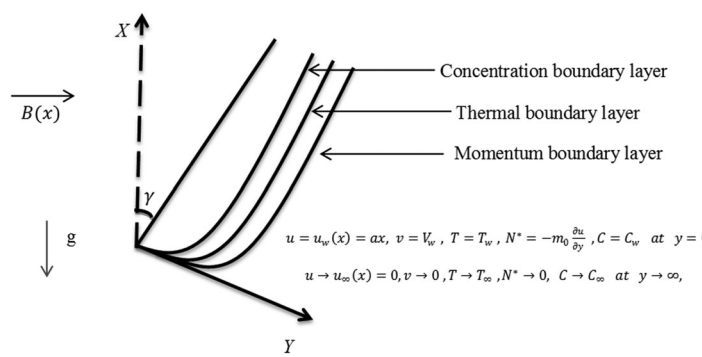

FIGURE 1 Physical geometry and coordinate system

The flow equations for this study are given as

$$\frac{\partial u}{\partial x}+\frac{\partial v}{\partial y}=0, \tag{1}$$

$$u\frac{\partial u}{\partial x}+v\frac{\partial u}{\partial y}=\left(\frac{\mu+K_1{}^*}{\rho}\right)\frac{\partial^2 u}{\partial y^2}+\left(\frac{K_1{}^*}{\rho}\right)\frac{\partial N^*}{\partial y}+g\left[\beta_t(T-T_\infty)+\beta_c(C-C_\infty)\right]\cos\gamma-\left(\frac{\sigma B_0^2}{\rho}\right)u, \tag{2}$$

$$u\frac{\partial N^*}{\partial x}+v\frac{\partial N^*}{\partial y}=\left(\frac{\gamma^*}{j^*\rho}\right)\frac{\partial^2 N^*}{\partial y^2}-\left(\frac{K_1{}^*}{j^*\rho}\right)\left(2N^*+\frac{\partial u}{\partial y}\right), \tag{3}$$

$$u\frac{\partial T}{\partial x}+v\frac{\partial T}{\partial y}=\alpha\frac{\partial^2 T}{\partial y^2}+\tau\left[D_B\frac{\partial C}{\partial y}\frac{\partial T}{\partial y}+\frac{D_T}{T_\infty}\left(\frac{\partial T}{\partial y}\right)^2\right]+\frac{D_T K_T}{C_s C_p}\frac{\partial^2 C}{\partial y^2}, \tag{4}$$

$$u\frac{\partial C}{\partial x}+v\frac{\partial C}{\partial y}=D_B\frac{\partial^2 C}{\partial y^2}+\frac{D_T K_T}{T_\infty}\frac{\partial^2 T}{\partial y^2}, \tag{5}$$

where u and v are the components of velocity in x and y directions, respectively, g is the acceleration due to gravity, B_0 is the uniform magnetic field strength, σdenotes the electrical conductivity, μ is the viscosity, ρ_f is the density of the base fluid, ρ_p denotes the density of the nanoparticle, $k_1{}^*$ is the vortex viscosity, β_t is the coefficient of thermal expansion, β_c denotes the coefficient of concentration expansion, γ^* is the spin gradient viscidness, the microinertia per unit mass is denoted by j^*, the angular velocity is denoted by N^*, D_B denotes the Brownian diffusion coefficient and D_T denotes the thermophoresis diffusion factor, k is the thermal conductivity, $(\rho c)_p$ denotes the heat capacitance of the nanoparticles, $(\rho c)_f$ represents the heat capacitance of the regular liquid, thermal diffusivity parameter is denoted by $\alpha=\frac{k}{(\rho c)_f}$, and the relation among the effective heat capacity of the nanoparticle and heat capacity of the liquid is represented by $\tau=\frac{(\rho c)_p}{(\rho c)_f}$.

The subjected boundary conditions are as follows:

$$u=u_w(x)=ax, v=V_w, T=T_w, N^*=-m_0\frac{\partial u}{\partial y}, C=C_w \quad \text{at } y=0, u\to u_\infty(x)=0, v\to 0,$$
$$T\to T_\infty, N^*\to 0, C\to C_\infty \quad \text{at } y\to\infty. \tag{6}$$

Here, the stream function $\psi=\psi(x,y)$ is demarcated as

$$u=\frac{\partial\psi}{\partial y}, v=-\frac{\partial\psi}{\partial x}, \tag{7}$$

where equation of continuity in Equation (1) is fulfilled. The similarity transformations are defined as

$$u=axf'(\eta), v=-\sqrt{av}f(\eta), \eta=y\sqrt{\frac{a}{v}},$$

$$\theta(\eta) = \frac{T - T_\infty}{T_w - T_\infty}, \phi(\eta) = \frac{C - C_\infty}{C_w - C_\infty}. \tag{8}$$

On substituting Equation (8), system of equations (2) to (5) are converted to

$$(1 + k)f''' + ff'' - f'^2 + kh' + (Gr_x\theta + Gc_x\phi)\cos\gamma - Mf' = 0, \tag{9}$$

$$\left(1 + \frac{k}{2}\right)h'' + fh' - f'h - k(2h + f'') = 0, \tag{10}$$

$$\left(\frac{1}{Pr}\right)\theta'' + f\theta' + Nb\phi'\theta' + Nt\theta'^2 + D_f\phi'' = 0, \tag{11}$$

$$\phi'' + Lef\phi' + SrLe\theta'' = 0, \tag{12}$$

where

$$M = \frac{\sigma B_0^2}{a\rho}, Le = \frac{\nu}{D_B}, Pr = \frac{\nu}{\alpha}, N_b = \frac{\tau D_B(C_w - C_\infty)}{\nu}, N_t = \frac{\tau D_t(T_w - T_\infty)}{\nu T_\infty},$$
$$Gr_x = \frac{g\beta_t(T_w - T_\infty)x^{-1}}{a^2}, Re = \frac{u_w x}{\nu}, Gc_x = \frac{g\beta_c(C_w - C_\infty)x^{-1}}{a^2}, D_f = \frac{D_T K_T(C_w - C_\infty)}{\nu C_s C_p(T_w - T_\infty)},$$
$$Sr = \frac{D_T K_T(T_w - T_\infty)}{\nu T_\infty(C_w - C_\infty)}. \tag{13}$$

Here, primes denote the differentiation with respect to η, M denotes the magnetic factor called Hartmann number, ν denotes the kinematic viscosity of the liquid, Pr denotes the Prandtl number, Lewis number is denoted by Le, the permeability parameter is represented by K, D_f is the Dufour factor, and Sr indicates the Soret factor. In addition, Gr_x signifies the local Grashof number, Gc_x denotes the local modified Grashof number, in order to make local Grashof number and local modified Grashof number free from x the coefficient of thermal expension β_t and coefficient of concentration expension β_c are proportional to x^1. Hence according to Makinde and Olanrewaju[39] and Rafique et al,[37] we assume that

$$\beta_t = nx^1, \beta_c = n_1x^1. \tag{14}$$

Here, n and n_1 are constants, thus Gr_x and Gc_x become

$$Gr = \frac{gn(T_w - T_\infty)}{a^2}, Gc = \frac{gn_1(C_w - C_\infty)}{a^2}. \tag{15}$$

The corresponding boundary settings are changed to

$$f(\eta) = S, f'(\eta) = 1, h(\eta) = 0, \theta(\eta) = 1, \phi(\eta) = 1, \text{ at } \eta = 0, f'(\eta) \to 0, h(\eta) \to 0,$$
$$\theta(\eta) \to 0, \phi(\eta) \to 0 \text{ as } \eta \to \infty. \tag{16}$$

It is found that by eliminating the vertex viscosity, that is, $K = 0$, it agrees to a nanofluid model deprived of micropolar effects. The skin friction, Sherwood number, and Nusselt number for the current study are defined as

$$Nu_x = \frac{xq_w}{k(T_w - T_\infty)}, Sh_x = \frac{xq_m}{D_B(C_w - C_\infty)}, C_f = \frac{t_w}{\frac{1}{2}u_w{}^2\rho_f}, \tag{17}$$

The related expressions for the skin-friction coefficient $C_{fx}(0) = f''(0)$, the reduced Sherwood number $-\phi'(0)$, and the reduced Nusselt number $-\theta'(0)$ are demarcated as

$$-\theta'(0) = \frac{Nu_x}{\sqrt{Re}}, -\phi'(0) = \frac{Sh_x}{\sqrt{Re}}, C_{fx} = C_f\sqrt{Re}, \tag{18}$$

where $Re = \frac{u_w x}{\nu}$ is the local Reynolds number.

The converted nonlinear differential equations (9) to (12) with the boundary settings (16) are elucidated by the Keller-Box scheme consisting of the steps as, finite-differences technique, Newton's procedure, and block elimination scheme clearly explained by Anwar et al.[31] In this study, step size $\Delta\eta = 0.01$ with boundary layer thickness $\eta_\infty = 10$ is considered. In addition, convergence criteria in this investigation depend on difference between current and previous iteration. The iteration process was terminated when convergence criterion 10^{-5} is satisfied for all points in η direction. The complete numerical scheme for this problem presented in Appendix A.

3 | RESULTS AND DISCUSSION

This bit of study deals with the determined consequences of changed over nonlinear ordinary differential equations (9) to (12) with boundary settings (16) elucidated by means of Keller-Box technique. For numerical outcome of physical parameters of our concern including Brownian motion parameter Nb, thermophoresis parameter Nt, magnetic factor M, local Grashof number Gr, local modified Grashof number Gc, inclination factor γ, Prandtl number Pr, Lewis number Le, Dufour effect D_f, Soret effect Sr, and material factor K, several figures and tables are prepared. In Table 1, in the deficiency of Dufour effect D_f, Soret effect Sr, buoyancy parameter λ, solutal buoyancy constraint δ, magnetic factor M, suction or injection parameter S, and

TABLE 1 Comparison of the reduced Nusselt number $-\theta'(0)$ and the reduced Sherwood number $-\phi'(0)$ when M, K, Sr, D_f, Gr, $Gc = 0$, $Pr =$, $Le = 10$, and $\gamma = 90°$

		Khan and Pop[40]		Present results	
Nb	***Nt***	$-\theta'(0)$	$-\phi'(0)$	$-\theta'(0)$	$-\phi'(0)$
0.1	0.1	0.9524	2.1294	0.9524	2.1294
0.2	0.2	0.3654	2.5152	0.3654	2.5152
0.3	0.3	0.1355	2.6088	0.1355	2.6088
0.4	0.4	0.0495	2.6038	0.0495	2.6038
0.5	0.5	0.0179	2.5731	0.0179	2.5731

TABLE 2 Values of the reduced Nusselt number $-\theta'(0)$, the reduced Sherwood number $-\phi'(0)$, and the skin-friction coefficient $C_{fx}(0)$

Nb	*Nt*	*Pr*	*Le*	*M*	*K*	*Gr*	*Gc*	*Sr*	D_f	*S*	γ	$-\theta'(0)$	$-\phi'(0)$	$C_{fx}(0)$
0.1	0.1	6.5	5.0	0.1	1.0	0.1	0.9	1.0	1.1	0.1	45°	0.5160	0.4916	0.9221
0.5	0.1	6.5	5.0	0.1	1.0	0.1	0.9	1.0	1.1	0.1	45°	0.5892	0.4004	0.8758
0.1	0.5	6.5	5.0	0.1	1.0	0.1	0.9	1.0	1.1	0.1	45°	0.3881	0.4191	0.9338
0.1	0.1	10.0	5.0	0.1	1.0	0.1	0.9	1.0	1.1	0.1	45°	0.5131	0.5016	0.9314
0.1	0.1	6.5	10.0	0.1	1.0	0.1	0.9	1.0	1.1	0.1	45°	0.5658	0.4918	0.9097
0.1	0.1	6.5	5.0	0.5	1.0	0.1	0.9	1.0	1.1	0.1	45°	0.4930	0.4707	1.1749
0.1	0.1	6.5	5.0	0.1	5.0	0.1	0.9	1.0	1.1	0.1	45°	0.5548	0.5265	1.6817
0.1	0.1	6.5	5.0	0.1	1.0	0.5	0.9	1.0	1.1	0.1	45°	0.5297	0.5041	0.7499
0.1	0.1	6.5	5.0	0.1	1.0	0.1	2.0	1.0	1.1	0.1	45°	0.5472	0.5201	0.4678
0.1	0.1	6.5	5.0	0.1	1.0	0.1	0.9	5.0	1.1	0.1	45°	0.2062	0.4121	0.9471
0.1	0.1	6.5	5.0	0.1	1.0	0.1	0.9	1.0	5.0	0.1	45°	0.5854	0.2741	0.7506
0.1	0.1	6.5	5.0	0.1	1.0	0.1	0.9	1.0	1.1	0.5	45°	0.3668	0.3328	0.7235
0.1	0.1	6.5	5.0	0.1	1.0	0.1	0.9	1.0	1.1	0.1	90°	0.4725	0.4520	1.3852

material factor K with $\gamma = 90°$ outcomes of reduced Nusselt number $-\theta'(0)$, reduced Sherwood number $-\phi'(0)$ are equated by existing outcomes of Khan and Pop.[40] The consequences are established brilliant settlement. The effects of $-\theta'(0)$, $-\phi'(0)$, and $C_{fx}(0)$, beside changed values of involved physical parameters Nb, Nt, M, K, Gr, Gc, γ, S, Le, D_f Sr, and Pr are shown in Table 2. From Table 2, it is clearly seen that $-\theta'(0)$ declines for growing the values of Nt, M, Le, Pr, Sr, S, γ, and increased by enhancing the numerical values of Nb, Le, Gr, D_f, Gc, and K.

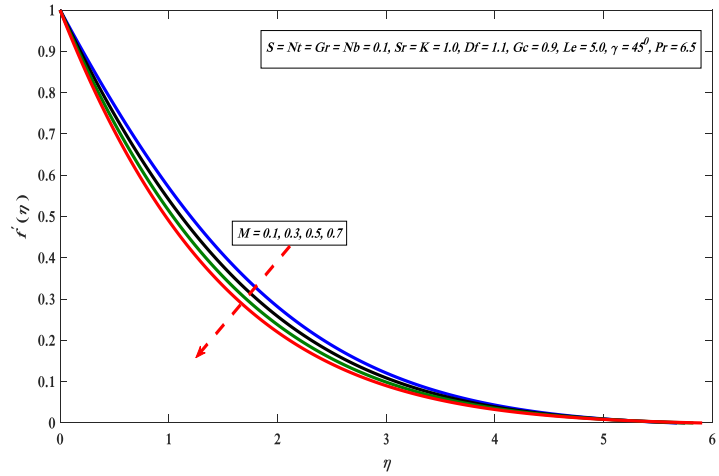

FIGURE 2 Variations in velocity profile for different values of M [Color figure can be viewed at wileyonlinelibrary.com]

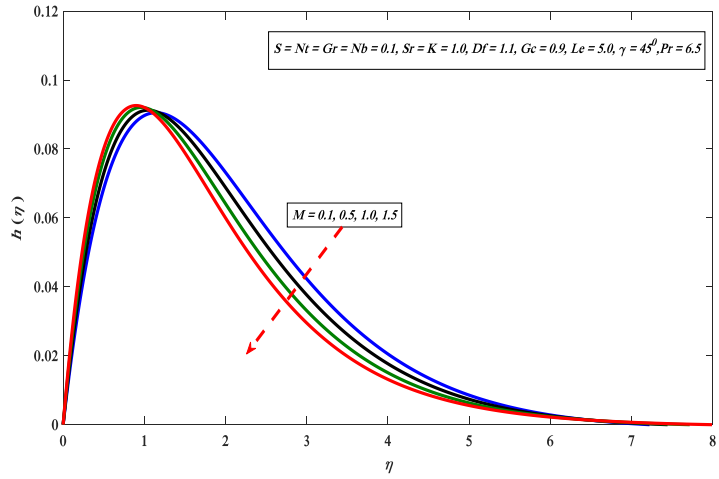

FIGURE 3 Variations in angular velocity profile for different value of M [Color figure can be viewed at wileyonlinelibrary.com]

Moreover, it is perceived that $-\phi'(0)$ enhanced with the larger values of Gr, Gc, Le, Pr, and drops for bigger values of Nt, Nb, M, S, K, D_f, Sr, and γ. Physically, due to the increment in Brownian motion factor Nb thermal boundary layer thickness increases affecting a large extent of fluid. While, Nusselt number and Sherwood number suppressed due to thermophoretic effects reason behind thermal boundary layer thicker due to deeper diffusion penetration into the fluid. On the other hand, $C_{fx}(0)$ rises with the growing values of Nt, M, K, Pr, Sr, γ, and drops with the higher values of, Le, Nb, Gr, Gc, S, and D_f.

A picture of the effect of factor M on velocity profile is portrayed in Figure 2. According to Figure 2 by improving the constraint M, the velocity outline reduces. Since magnetic field produces Lorentz force, by means slow down the speed of the liquid. The

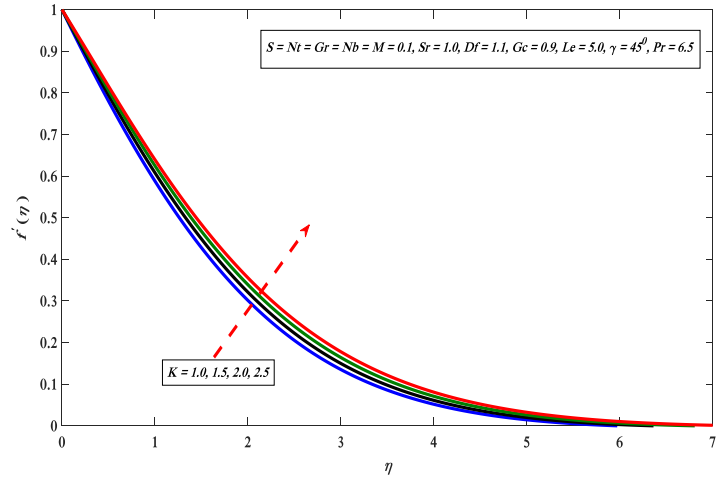

FIGURE 4 Variations in velocity profile for different values of K [Color figure can be viewed at wileyonlinelibrary.com]

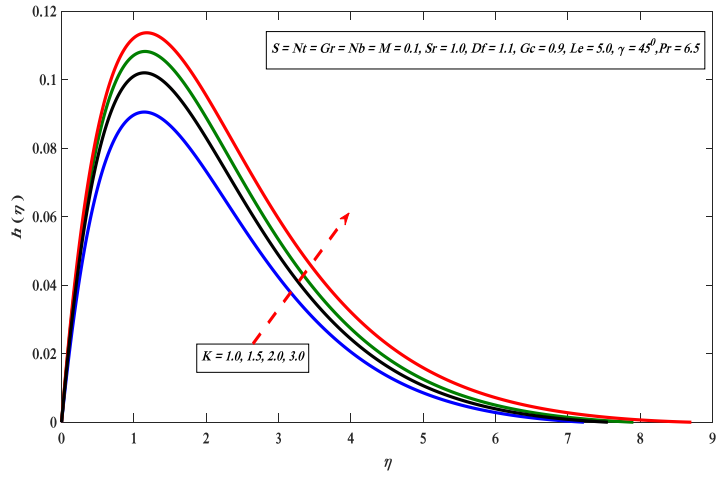

FIGURE 5 Variations in angular velocity profile for different values of K [Color figure can be viewed at wileyonlinelibrary.com]

parallel outcome has gotten in the instance of angular velocity against changed values of M in Figure 3. The velocity profile upturn by improving the values of K is exposed in Figure 4. Besides, Figure 5 points out that the angular velocity profile upsurge by growing factor K. Physically, viscidness of the boundary layer losses by improving the values of K. The impact of Gr on velocity profile is displayed in Figure 6. It demonstrates that the velocity contour enhanced for changed values of Gr. Physically, increment in buoyancy forces decreases the viscous force, which is favorable to the fluid motion. Figure 7 portrayed the effect of Gc on velocity profile. It is noted from Figure 7 the velocity profile

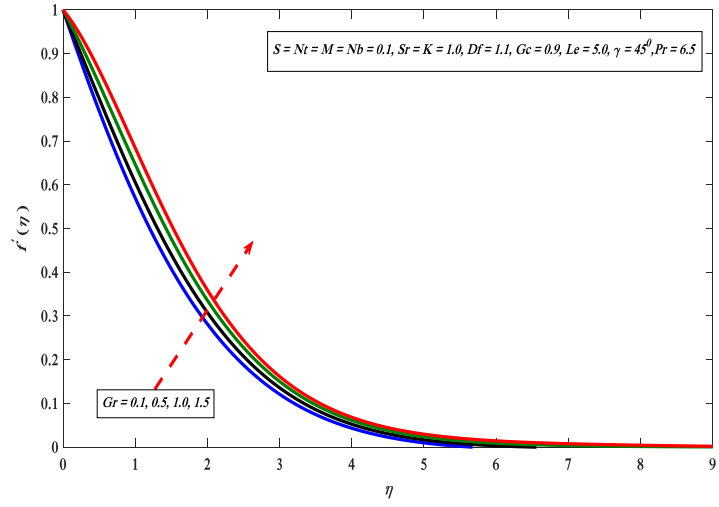

FIGURE 6 Variations in velocity profile for different values of Gr [Color figure can be viewed at wileyonlinelibrary.com]

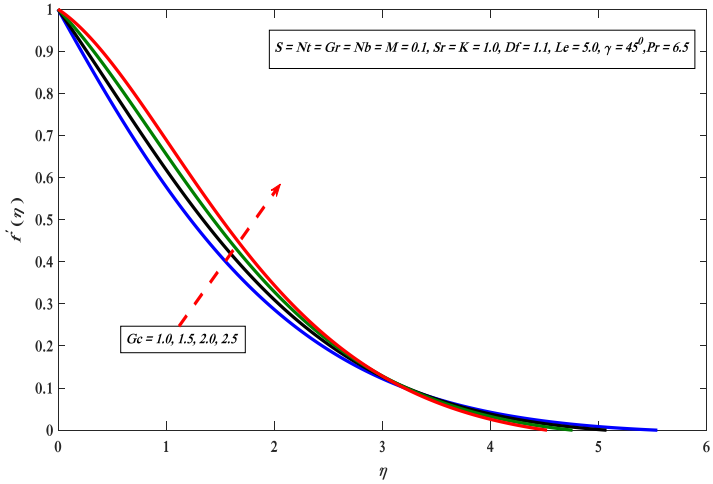

FIGURE 7 Variations in velocity profile for different values of *Gc* [Color figure can be viewed at wileyonlinelibrary.com]

upturn by enhancing the constraint *Gc*. Physically, the viscosity of the liquid falls with the growth of *Gc*, and the concentration upturns, which reasons the enhancement in velocity contour. Figure 8 interprets the significance of inclination factor γ on velocity outline. It is perceived from Figure 8 that velocity outline runs down by enhancing the values of γ. Moreover, the circumstances indicate that the maximum gravitational force act on flow in the case of $\gamma = 0$ because in this state, the sheet will be vertical. On the other hand, for $\gamma = 90^{o}$, the sheet will be horizontal, which causes the decline in velocity profile as the

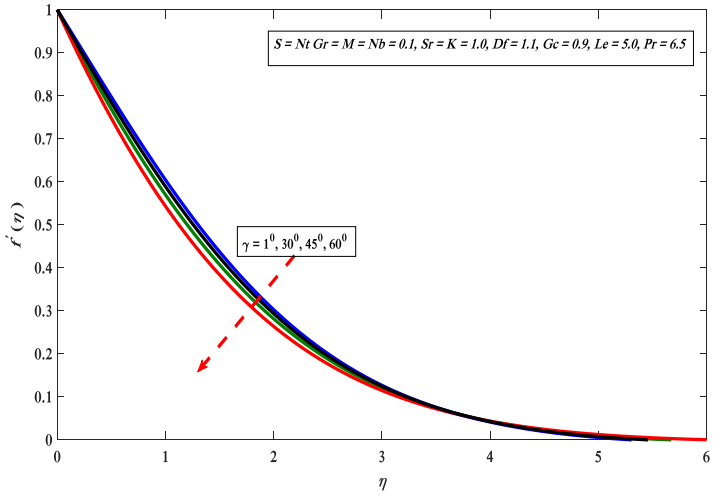

FIGURE 8 Variations in velocity profile for different values of γ [Color figure can be viewed at wileyonlinelibrary.com]

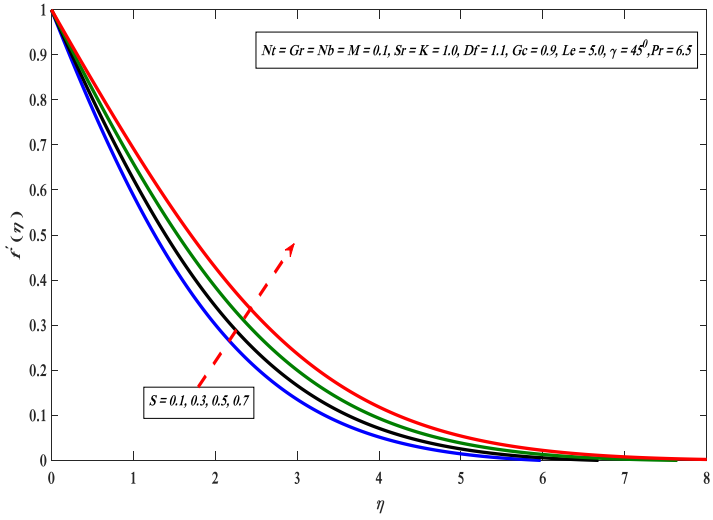

FIGURE 9 Variations in velocity profile for different values of S [Color figure can be viewed at wileyonlinelibrary.com]

power of the bouncy forces drop. Whereas Figure 9 presented that the velocity profile enhanced against large values of suction or injection parameter S reason behind lessening the boundary layer thickness. The impact of Figure 10 shows that the temperature profile falls against growing values of D_f. Physically, the boundary layer thickness decreases with the effect of Dufour number on nanofluid motion due to which the heat exchange enhanced. Whereas, concentration profile turns up for higher values of Sr in Figure 11. On the other hand, concentration profile falls down in Figure 12 for large values of Le because Lewis number diminishes the boundary layer thickness.

FIGURE 10 Variations in temperature profile for different values of D_f [Color figure can be viewed at wileyonlinelibrary.com]

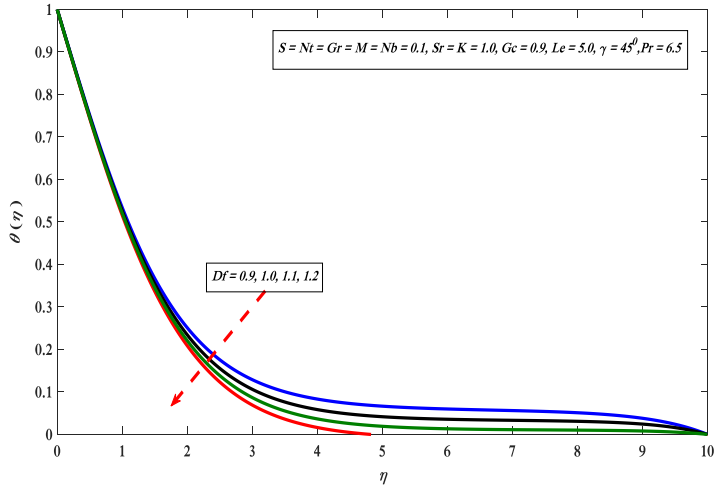

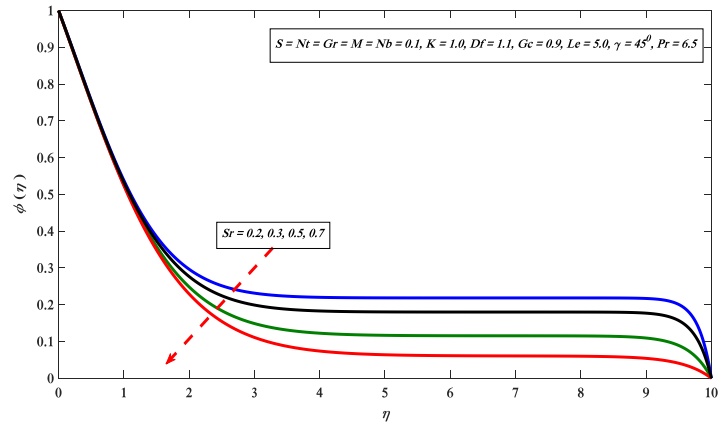

FIGURE 11 Variations in concentration profile for different values of *Sr* [Color figure can be viewed at wileyonlinelibrary.com]

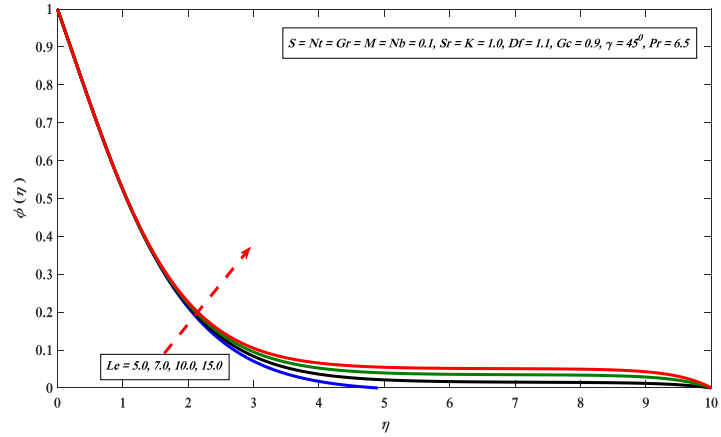

FIGURE 12 Variation in concentration profile for different values of *Le* [Color figure can be viewed at wileyonlinelibrary.com]

4 | CONCLUSIONS

This study explored the heat and mass exchange of micropolar nanofluid flow over a linear permeable inclined extending sheet. The Brownian motion and thermophoresis effects are taken into account. The numerical results are obtained via the Keller-Box scheme and compared with already published literature.[40] In this problem, heat and mass transfer phenomenon was discussed numerically. The main findings of this study are as follows.

1. Energy and mass transfer rates decrease with the increment in inclination factor.
2. The concentration profile decreases with the growth of the Soret effect.
3. Dufour effect diminishes temperature profile.
4. Table 2 presented that Nusselt and Sherwood numbers reduce by increasing the magnetic effect.

5. The velocity profile increases with enhancement in local Grashof number and local modified Grashof number.

ORCID

Muhammad Imran Asjad http://orcid.org/0000-0002-1484-5114

REFERENCES

1. Sakiadis BC. Boundary-layer behavior on continuous solid surfaces: I. Boundary-layer equations for two-dimensional and axisymmetric flow. *AIChE J*. 1961;7(1):26-28.
2. Crane LJ. Flow past a stretching plate. *Zeitschrift Für Angewandte Mathematik Und Physik*. 1970;21(4):645-647.
3. Noor NFM, Abbasbandy S, Hashim I. Heat and mass transfer of thermophoretic MHD flow over an inclined radiate isothermal permeable surface in the presence of heat source/sink. *Int J Heat Mass Transfer*. 2012;55(7–8):2122-2128.
4. Tshehla MS. The flow of a variable viscosity fluid down an inclined plane with a free surface. *Math Probl Eng*. 2013;2013:754782.
5. Bognár G, Gombkötő I, Hriczó K. Non-Newtonian fluid flow down an inclined plane. In: 9th ASME/WSEAS International Conference on Fluid Mechanics and Aerodynamics, Florence, Italy; 2011:23-25.
6. Hamza MA, Jameel AT, Asrar W, Hoda A. Numerical simulation of non-isothermal thin liquid film flow on inclined plane using an implicit finite difference scheme. *IOP Conf Ser, Mat Sci Eng*. 2017;184:12004.
7. Raju RS. Unsteady MHD boundary layer flow of Casson fluid over an inclined surface embedded in a porous medium with thermal radiation and chemical reaction. *J Nanofluids*. 2018;7(4):694-703.
8. Reddy VR, Reddy MS, Nagendra N, Rao AS, Reddy MS. Radiation effect on boundary layer flow of a non Newtonian Jeffrey fluid past an inclined vertical plate. *I-Manage J Math*. 2017;6(2):34.
9. Singh PK. Heat and mass transfer in MHD boundary layer flow past an inclined plate with viscous dissipation in porous medium. *Int J Sci Eng Res*. 2012;3(6):1-11.
10. Das SK, Choi SU, Yu W, Pradeep T. *Nanofluids: science and technology*. Hoboken, NJ: John Wiley & Sons; 2007.
11. Buongiorno J. Convective transport in nanofluids. *J Heat Transfer*. 2006;128(3):240-250.
12. Sandeep N, Kumar MS. Heat and mass transfer in nanofluid flow over an inclined stretching sheet with volume fraction of dust and nanoparticles. *J Appl Fluid Mech*. 2016;9(5):2205-2215.
13. Rashad AM. Unsteady nanofluid flow over an inclined stretching surface with convective boundary condition and anisotropic slip impact. *Int J Heat Technol*. 2017;35(1):82-90.
14. Govindarajan A. Radiative fluid flow of a nanofluid over an inclined plate with non-uniform surface temperature. *J Phys, Conf Ser*. 2018;1000:12173.
15. Suriyakumar P, Devi SPA. Effects of suction and internal heat generation on hydromagnetic mixed convective nanofluid flow over an inclined stretching plate. *Eur J Adv Eng Technol*. 2015;2(3):51-58.
16. Khan I, Malik MY, Hussain A, Khan M. Magnetohydrodynamics Carreau nanofluid flow over an inclined convective heated stretching cylinder with Joule heating. *Results Phys*. 2017;7:4001-4012.
17. Chakraborty T, Das K, Kundu PK. Ag-water nanofluid flow over an inclined porous plate embedded in a non-Darcy porous medium due to solar radiation. *J Mech Sci Technol*. 2017;31(5):2443-2449. https://doi.org/10.1007/s12206-017-0442-4
18. Ziaei-Rad M, Kasaeipoor A, Rashidi MM, Lorenzini G. A similarity solution for mixed-convection boundary layer nanofluid flow on an inclined permeable surface. *J Therm Sci Eng Appl*. 2017;9(2):21015.
19. Afify AA. The influence of slip boundary condition on Casson nanofluid flow over a stretching sheet in the presence of viscous dissipation and chemical reaction. *Math Probl Eng*. 2017;2017:3804751.
20. Halim NA, Sivasankaran S, Noor NM. Active and passive controls of the Williamson stagnation nanofluid flow over a stretching/shrinking surface. *Neural Comput Appl*. 2017;28(1):1023-1033.
21. Sher Akbar N, Nadeem S, M Noor NF. Free convective MHD peristaltic flow of a Jeffrey nanofluid with convective surface boundary condition: a biomedicine--nano model. *Curr Nanosci*. 2014;10(3):432-440.
22. Rafique K, Anwar MI, Misiran M, et al. Numerical solution of Casson nanofluid flow over a non-linear inclined surface with Soret and Dufour effects by Keller-Box method. *Front Phys*. 2019;7:139.

23. Bég OA, Bég TA, Bakier AY, Prasad VR. Chemically-reacting mixed convective heat and mass transfer along inclined and vertical plates with Soret and Dufour effects: numerical solutions. *Int J Appl Math Mech*. 2009; 5(2):39-57.
24. Pal D, Chatterjee S. Soret and Dufour effects on MHD convective heat and mass transfer of a power-law fluid over an inclined plate with variable thermal conductivity in a porous medium. *Appl Math Comput*. 2013; 219(14):7556-7574. https://doi.org/10.1016/j.amc.2012.10.119
25. Balla CS, Naikoti K. Soret and Dufour effects on free convective heat and solute transfer in fluid saturated inclined porous cavity. *Eng Sci Technol, Int J*. 2015;18(4):543-554.
26. Sravanthi CS. Homotopy analysis solution of MHD slip flow past an exponentially stretching inclined sheet with Soret-Dufour effects. *J Niger Math Soc*. 2016;35(1):208-226.
27. Eringen AC. Simple microfluids. *Int J Eng Sci*. 1964;2(2):205-217.
28. Rahman MM, Aziz A, Al-Lawatia MA. Heat transfer in micropolar fluid along an inclined permeable plate with variable fluid properties. *Int J Therm Sci*. 2010;49(6):993-1002. https://doi.org/10.1016/j.ijthermalsci.2010.01.002
29. Uddin MJ. Convective flow of micropolar fluids along an inclined flat plate with variable electric conductivity and uniform surface heat flux. *Daffodil Int Univ J Sci Technol*. 2011;6(1):69-79.
30. Das K. Slip effects on heat and mass transfer in MHD micropolar fluid flow over an inclined plate with thermal radiation and chemical reaction. *Int J Numer Methods Fluids*. 2012;70(1):96-113. https://doi.org/10.1002/fld.2683
31. Anwar MI, Shafie S, Hayat T, Shehzad SA, Salleh MZ. Numerical study for MHD stagnation-point flow of a micropolar nanofluid towards a stretching sheet. *J Braz Soc Mech Sci Eng*. 2017;39(1):89-100. https://doi.org/10.1007/s40430-016-0610-y
32. Hazbavi A, Sharhani S. Micropolar fluid flow between two inclined parallel plates. In: American Society of Mechanical Engineers International Mechanical Engineering Congress and Exposition; 2017.
33. Srinivasacharya D, RamReddy C, Naveen P. Double dispersion effect on nonlinear convective flow over an inclined plate in a micropolar fluid saturated non-Darcy porous medium. *Eng Sci Technol*. 2018;21:984-995.
34. Srinivasacharya D, Bindu KH. Entropy generation in a micropolar fluid flow through an inclined channel. *Alexandr Eng J*. 2016;55(2):973-982.
35. Shamshuddin MD, Mishra SR, Bég OA, Kadir A. Unsteady reactive magnetic radiative micropolar flow, heat and mass transfer from an inclined plate with joule heating: a model for magnetic polymer processing. *Proc Inst Mech Eng*. 2019;233(4):1246-1261.
36. Noor NFM, Haq RU, Nadeem S, Hashim I. Mixed convection stagnation flow of a micropolar nanofluid along a vertically stretching surface with slip effects. *Meccanica*. 2015;50(8):2007-2022.
37. Rafique K, Anwar MI, Misiran M, et al. Numerical analysis with Keller-Box scheme for stagnation point effect on flow of micropolar nanofluid over an inclined surface. *Symmetry*. 2019;11(11):1379.
38. Mishra SR, Baag S, Mohapatra DK. Chemical reaction and Soret effects on hydromagnetic micropolar fluid along a stretching sheet. *Eng Sci Technol, Int J*. 2016;19(4):1919-1928. https://doi.org/10.1016/j.jestch.2016.07.016
39. Makinde OD, Olanrewaju PO. Buoyancy effects on thermal boundary layer over a vertical plate with a convective surface boundary condition. *J Fluids Eng*. 2010;132(4):044502.
40. Khan WA, Pop I. Boundary-layer flow of a nanofluid past a stretching sheet. *Int J Heat Mass Transfer*. 2010; 53(11):2477-2483.

How to cite this article: Rafique K, Anwar MI, Misiran M, Asjad MI. Energy and mass transport of micropolar nanofluid flow over an inclined surface with Keller-Box simulation. *Heat Transfer*. 2020;1–20. https://doi.org/10.1002/htj.21843

APPENDIX A

see: Figure A1

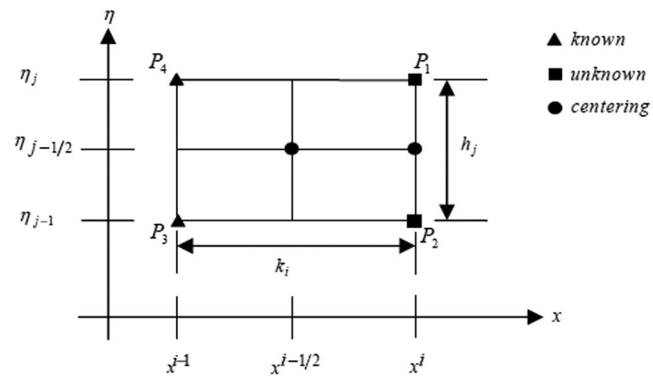

FIGURE A1 Net rectangle for difference approximations

A.1 | Numerical procedure

The numerical formulation of the Keller-Box method for the problem considered for micropolar nanofluid is explained for the finite-difference method, block-elimination method.

A.2 | The finite difference method

As described by Anwar et al,[31] Equations (9) to (12) subject to the boundary conditions (17) are written in a system of first-order differential equations. For this purpose, new dependent variables are introduced for $f(\eta)$, $u(\eta)$, $v(\eta)$, $g(\eta)$, $p(\eta)$, $q(\eta)$, and $s(\eta)$. Also, $\theta(\eta)$ and $\phi(\eta)$ are replaced with $g(\eta)$ and $q(\eta)$, respectively, which represent the fluid temperature and concentration respectively. Therefore, in the following first-order equations are

$$f'(\eta) = u(\eta), u'(\eta) = v(\eta), g'(\eta) = p(\eta), q'(\eta) = s(\eta), \tag{19}$$

$$(1 + k)v' + fv - u^2 + kl + (Grg - Gcq)\cos\gamma - Mu = 0, \tag{20}$$

$$\left(1 + \frac{k}{2}\right)l' + fl - ut - k(2t + v) = 0, \tag{21}$$

$$\left(\frac{1}{Pr}\right)p' + fp + Nbsp + Ntp^2 + D_f s' = 0, \tag{22}$$

$$s' + Lefs + SrLep' = 0. \tag{23}$$

The boundary conditions in terms of new dependent variable η, become

$$f(\eta) = S, u(\eta) = 1, h(\eta) = 0, g(\eta) = 1, q(\eta) = 1 \text{ at } \eta = 0 u(\eta) \to 0, h(\eta) = 0,$$
$$g(\eta) \to 0, q(\eta) \to 0 \text{ as } \eta \to \infty. \tag{24}$$

The net rectangle is considered in the x-η plane as shown in Figure A1 and the net points are defined as

$$x^0 = 0, x^i = x^{i-1} + k_i, i = 1, 2, 3, ...I, \tag{25}$$

$$\eta_0 = 0, \eta_j = \eta_{j-1} + h_j, j = 1, 2, 3, ...J, \eta_J \equiv \eta_\infty, \tag{26}$$

where k_i is the Δx–spacing and h_j is the $\Delta\eta$-spacing. Here, i and j are just sequence of numbers that indicate the coordinate location, not tensor indices or exponents.

The derivatives in the x-direction are given by finite difference, for example

$$\frac{\partial u}{\partial x} = \frac{u^i - u^{i-1}}{k_i}, \tag{27}$$

while the derivatives in the η-direction are replaced by finite difference, for example

$$v' = \frac{\partial v}{\partial \eta} = \frac{v_j - v_{j-1}}{h_j}, \tag{28}$$

for any points

$$()_j^{i-1/2} = \frac{1}{2}\left[()_j^i + ()_j^{i-1}\right], \tag{29}$$

and

$$()_{j-1/2}^i = \frac{1}{2}\left[()_j^i + ()_{j-1}^i\right]. \tag{30}$$

The difference equations, which are to approximate equations (a) are written by considering one mesh rectangle as shown in Figure A1. Using centered-difference derivatives, the finite difference approximations of the ordinary differential equations (a) are written for the midpoint ($\eta_{j\text{-}1/2}$) of the segment P_1P_2. This process is called "centering about ($\eta_{j\text{-}1/2}$)" written as

$$\begin{aligned}
\frac{\left(f_j^i - f_{j-1}^i\right)}{h_j} &= \frac{1}{2}\left(u_j^i - u_{j-1}^i\right) = u_{j-\frac{1}{2}}^i \frac{\left(u_j^i - u_{j-1}^i\right)}{h_j} = \frac{1}{2}\left(v_j^i - v_{j-1}^i\right) = v_{j-\frac{1}{2}}^i \frac{\left(t_j^i - t_{j-1}^i\right)}{h_j} \\
&= \frac{1}{2}\left(l_j^i - l_{j-1}^i\right) = l_{j-\frac{1}{2}}^i \frac{\left(g_j^i - g_{j-1}^i\right)}{h_j} = \frac{1}{2}\left(p_j^i - p_{j-1}^i\right) = p_{j-\frac{1}{2}}^i \frac{\left(q_j^i - q_{j-1}^i\right)}{h_j} \\
&= \frac{1}{2}\left(s_j^i - s_{j-1}^i\right) = s_{j-\frac{1}{2}}^i (1+k) \frac{\left(v_j^i - v_{j-1}^i\right)}{h_j} + \left[\left(\frac{\left(f_j^i - f_{j-1}^i\right)}{2}\right)\left(\frac{\left(v_j^i - v_{j-1}^i\right)}{2}\right)\right] \\
&\quad - \left(\frac{\left(u_j^i - u_{j-1}^i\right)}{2}\right)^2 + k\frac{\left(l_j^i - l_{j-1}^i\right)}{2} \\
&\quad + \left[Gr\left(\frac{\left(g_j^i - g_{j-1}^i\right)}{2}\right) - Gc\left(\frac{\left(q_j^i - q_{j-1}^i\right)}{2}\right)\right]\cos\gamma - M\frac{\left(u_j^i - u_{j-1}^i\right)}{2} \\
&= 0\left(1 + \frac{k}{2}\right)\frac{\left(l_j^i - l_{j-1}^i\right)}{h_j} + \left[\left(\frac{\left(f_j^i - f_{j-1}^i\right)}{2}\right)\left(\frac{\left(l_j^i - l_{j-1}^i\right)}{2}\right)\right] \\
&\quad - \left[\left(\frac{\left(u_j^i - u_{j-1}^i\right)}{2}\right)\left(\frac{\left(t_j^i - t_{j-1}^i\right)}{2}\right)\right] - k\left[2\left(\frac{\left(t_j^i - t_{j-1}^i\right)}{2}\right) + \left(\frac{\left(v_j^i - v_{j-1}^i\right)}{2}\right)\right] \\
&= 0\left(\frac{1}{Pr}\right)\frac{\left(p_j^i - p_{j-1}^i\right)}{h_j} + \left[\left(\frac{\left(f_j^i - f_{j-1}^i\right)}{2}\right)\left(\frac{\left(p_j^i - p_{j-1}^i\right)}{2}\right)\right] \\
&\quad + Nb\left[\left(\frac{\left(s_j^i - s_{j-1}^i\right)}{2}\right)\left(\frac{\left(p_j^i - p_{j-1}^i\right)}{2}\right)\right] + Nt\left[\left(\frac{\left(p_j^i - p_{j-1}^i\right)}{2}\right)^2\right] + D_f\frac{\left(s_j^i - s_{j-1}^i\right)}{h_j} \\
&= 0\frac{\left(s_j^i - s_{j-1}^i\right)}{h_j} + Le\left[\left(\frac{\left(f_j^i - f_{j-1}^i\right)}{2}\right)\left(\frac{\left(s_j^i - s_{j-1}^i\right)}{2}\right)\right] + SrLe\left[\left(\frac{\left(p_j^i - p_{j-1}^i\right)}{h_j}\right)\right] = 0.
\end{aligned} \tag{31}$$

At $x = x^i$, the subjected boundary conditions (24) in terms of the dependent variable (η) become

$$f_0^i = 0, u_0^i = 1, g_0^i = 1, q_0^i = 1, \tag{32}$$

$$u_J^i = 0, g_J^i = 0, q_J^i = 0. \tag{33}$$

A.3 | Newton's method

If $f_j^{i-1}, u_j^{i-1}, v_j^{i-1}, g_j^{i-1}, p_j^{i-1}, q_j^{i-1}, s_j^{i-1}$ are assumed to be known for $0 \le j \le J$, then the solution of the unknown $(f_j^i, u_j^i, v_j^i, g_j^i, p_j^i, q_j^i, s_j^i)$, $0 \le j \le J$, have to be obtained. For the simplicity of notations[31] and dropping the quadratic and higher order terms in $\delta f_j^k, \delta u_j^k, \delta v_j^k, \delta g_j^k, \delta p_j^k, \delta q_j^k$, and δs_j^k as well as the superscript i gives

$$\begin{aligned}
\delta f_j - \delta f_{j-1} - \frac{h_j}{2}(\delta u_j - \delta u_{j-1}) &= (r_1)_{j-\frac{1}{2}}\delta u_j - \delta u_{j-1} - \frac{h_j}{2}(\delta v_j - \delta v_{j-1}) \\
&= (r_2)_{j-\frac{1}{2}}\delta t_j - \delta t_{j-1} - \frac{h_j}{2}(\delta l_j - \delta l_{j-1}) \\
&= (r_3)_{j-\frac{1}{2}}\delta g_j - \delta g_{j-1} - \frac{h_j}{2}(\delta p_j - \delta p_{j-1}) \\
&= (r_4)_{j-\frac{1}{2}}\delta q_j - \delta q_{j-1} - \frac{h_j}{2}(\delta s_j - \delta s_{j-1}) \\
&= (r_5)_{j-\frac{1}{2}}(a_1)_j\delta v_j + (a_2)_j\delta v_{j-1} + (a_3)_j\delta f_j + (a_4)_j\delta f_{j-1} + (a_5)_j\delta u_j \\
&\quad + (a_6)_j\delta u_{j-1} + (a_7)_j\delta l_j + (a_8)_j\delta l_{j-1} + (a_9)_j\delta g_j + (a_{10})_j\delta g_{j-1} \\
&\quad + (a_{11})_j\delta q_j + (a_{12})_j\delta q_{j-1} = (r_6)_{j-\frac{1}{2}}(b_1)_j\delta l_j + (b_2)_j\delta l_{j-1} \\
&\quad + (b_3)_j\delta f_j + (b_4)_j\delta f_{j-1} + (b_5)_j\delta u_j + (b_6)_j\delta u_{j-1} + (b_7)_j\delta v_j \\
&\quad + (b_8)_j\delta v_{j-1} + (b_9)_j\delta t_j + (b_{10})_j\delta t_{j-1} \\
&= (r_7)_{j-\frac{1}{2}}(c_1)_j\delta p_j + (c_2)_j\delta p_{j-1} + (c_3)_j\delta f_j + (c_4)_j\delta f_{j-1} + (c_5)_j\delta s_j \\
&\quad + (c_6)_j\delta s_{j-1} = (r_8)_{j-\frac{1}{2}}(d_1)_j\delta s_j + (d_2)_j\delta s_{j-1} + (d_3)_j\delta f_j \\
&\quad + (d_4)_j\delta f_{j-1} + (d_5)_j\delta p_j + (d_6)_j\delta p_{j-1} = (r_9)_{j-\frac{1}{2}},
\end{aligned} \tag{34}$$

where

$$\begin{aligned}
(a_1)_j &= 1 + k + \frac{h_j}{2}f_{j-\frac{1}{2}}, (a_2)_j = -(1+k) + \frac{h_j}{2}f_{j-\frac{1}{2}}, (a_3)_j = \frac{h_j}{2}v_{j-\frac{1}{2}}, (a_3)_j = (a_4)_j, (a_5)_j \\
&= h_j u_{j-\frac{1}{2}} - h_j M, (a_5)_j = (a_6)_j, (a_7)_j = \frac{kh_j}{2}, (a_7)_j = (a_8)_j, (a_9)_j \\
&= (Gr)h_j\cos\alpha, (a_9)_j = (a_{10})_j(a_{11})_j = (Gc)h_j\cos\alpha, (a_{11})_j = (a_{12})_j(b_1)_j \\
&= 1 + \frac{k}{2} + \frac{h_j}{2}f_{j-\frac{1}{2}}, (b_2)_j = -\left(1 + \frac{k}{2}\right) + \frac{h_j}{2}f_{j-\frac{1}{2}}, (b_3)_j = \frac{h_j}{2}l_{j-\frac{1}{2}}, (b_3)_j = (b_4)_j, (b_5)_j \\
&= \frac{-h_j}{2}u_{j-\frac{1}{2}} - kh_j, (b_5)_j = (b_6)_j, (b_7)_j = \frac{-h_j}{2}t_{j-\frac{1}{2}}, (b_7)_j = (b_8)_j, (b_9)_j = -kh_j, (b_9)_j \\
&= (b_{10})_j(c_1)_j = 1 + Pr\frac{h_j}{2}f_{j-\frac{1}{2}} + \frac{NbPrh_j}{2}s_{j-\frac{1}{2}} + h_j NtPrp_{j-\frac{1}{2}}, (c_2)_j = (c_1)_j - 2, (c_3)_j \\
&= Pr\frac{h_j}{2}p_{j-\frac{1}{2}}, (c_3)_j = (c_4)_j, (c_5)_j = \frac{NbPrh_j}{2}p_{j-\frac{1}{2}}, (c_5)_j = (c_6)_j, (c_7)_j = D_f h_j, (c_8)_j = -(c_7)_j(d_1)_j \\
&= 1 + \frac{h_j Le}{2}f_{j-\frac{1}{2}}, (d_2)_j = (d_1)_j - 2, (d_3)_j = \frac{Leh_j}{2}s_{j-\frac{1}{2}}, (d_3)_j = (d_4)_j, (d_5)_j = LeSr, (d_6)_j \\
&= -LeSr.
\end{aligned}$$

The boundary conditions are

$$\delta f_0 = 0, \delta u_0 = 0, \delta h_0 = 0, \delta g_0 = 0, \delta q_0 = 0, \delta u_j = 0, \delta h_0 = 0, \delta g_j = 0, \delta q_j = 0. \tag{35}$$

A.4 | The block-elimination method

The linearized differential equations of the system (34) have a block-tridiagonal structure.[31] In vector-matrix form, it can be written as

$$[A][\delta] = [r], \tag{36}$$

where

$$[A] = \begin{bmatrix} [A_1] & [C_1] & & & & \\ [B_2] & [A_2] & [C_2] & & & \\ & & \ddots & & & \\ & & & \ddots & & \\ & & & & \ddots & \\ & & & [B_{J-1}] & [A_{J-1}] & [C_{J-1}] \\ & & & & [B_J] & [C_J] \end{bmatrix}, \quad [\delta] = \begin{bmatrix} [\delta_1] \\ [\delta_2] \\ \vdots \\ [\delta_{J-1}] \\ [\delta_J] \end{bmatrix}, \quad [r] = \begin{bmatrix} [r_1] \\ [r_2] \\ \vdots \\ [r_{J-1}] \\ [r_J] \end{bmatrix}. \tag{37}$$

The block-tridiagonal structure are commonly consisting of variables or constants, but here, an interesting feature can be observed that is, for the Keller-Box method, it consists of block matrices. By taking $K = 1$, $M = 1$, the elements of matrices are defined as follows:

where $e_1 = \frac{-h_1}{2}$

$$[A_1] = \begin{bmatrix} 0 & 0 & 0 & 0 & 1 & 0 & 0 & 0 & 0 \\ \frac{-h_2}{2} & 0 & 0 & 0 & 0 & \frac{-h_2}{2} & 0 & 0 & 0 \\ 0 & \frac{-h_2}{2} & 0 & 0 & 0 & 0 & \frac{-h_2}{2} & 0 & 0 \\ 0 & 0 & \frac{-h_2}{2} & 0 & 0 & 0 & 0 & \frac{-h_2}{2} & 0 \\ 0 & 0 & 0 & \frac{-h_2}{2} & 0 & 0 & 0 & 0 & \frac{-h_2}{2} \\ (a_2)_1 & (a_8)_1 & 0 & 0 & (a_3)_1 & (a_1)_1 & (a_7)_1 & 0 & 0 \\ (b_8)_1 & (b_2)_1 & 0 & 0 & (b_3)_1 & (b_7)_1 & (b_1)_1 & 0 & 0 \\ 0 & 0 & (c_2)_1 & (c_6)_1 & (c_3)_1 & 0 & 0 & (c_1)_1 & (c_5)_1 \\ 0 & 0 & (d_6)_1 & (d_2)_1 & (d_3)_1 & 0 & 0 & (d_5)_1 & (d_1)_1 \end{bmatrix}, \tag{38}$$

$$[A_j] = \begin{bmatrix} e_j & 0 & 0 & 0 & 1 & 0 & 0 & 0 & 0 \\ -1 & 0 & 0 & 0 & 0 & e_j & 0 & 0 & 0 \\ 0 & -1 & 0 & 0 & 0 & 0 & e_j & 0 & 0 \\ 0 & 0 & -1 & 0 & 0 & 0 & 0 & e_j & 0 \\ 0 & 0 & 0 & -1 & 0 & 0 & 0 & 0 & e_j \\ (a_6)_j & 0 & (a_{10})_j & (a_{12})_j & (a_3)_j & (a_1)_j & (a_7)_j & 0 & 0 \\ (b_6)_j & (b_{10})_j & 0 & 0 & (b_3)_j & (b_7)_j & (b_1)_j & 0 & 0 \\ 0 & 0 & 0 & 0 & (c_3)_j & 0 & 0 & (c_1)_j & (c_5)_j \\ 0 & 0 & 0 & 0 & (d_3)_j & 0 & 0 & (d_5)_j & (d_1)_j \end{bmatrix}, \tag{39}$$

$$[B_j] = \begin{bmatrix} 0 & 0 & 0 & 0 & -1 & 0 & 0 & 0 & 0 \\ 0 & 0 & 0 & 0 & 0 & e_j & 0 & 0 & 0 \\ 0 & 0 & 0 & 0 & 0 & 0 & e_j & 0 & 0 \\ 0 & 0 & 0 & 0 & 0 & 0 & 0 & e_j & 0 \\ 0 & 0 & 0 & 0 & 0 & 0 & 0 & 0 & e_j \\ 0 & 0 & 0 & 0 & (a_4)_j & (a_2)_j & (a_8)_j & 0 & 0 \\ 0 & 0 & 0 & 0 & (b_4)_j & (b_8)_j & (b_2)_j & 0 & 0 \\ 0 & 0 & 0 & 0 & (c_4)_j & 0 & 0 & (c_2)_j & (c_8)_j \\ 0 & 0 & 0 & 0 & (d_4)_j & 0 & 0 & (d_6)_j & (d_2)_j \end{bmatrix} \quad 2 \le j \le J, \tag{40}$$

$$[C_j] = \begin{bmatrix} e_j & 0 & 0 & 0 & 0 & 0 & 0 & 0 & 0 \\ 1 & 0 & 0 & 0 & 0 & 0 & 0 & 0 & 0 \\ 0 & 1 & 0 & 0 & 0 & 0 & 0 & 0 & 0 \\ 0 & 0 & 1 & 0 & 0 & 0 & 0 & 0 & 0 \\ 0 & 0 & 0 & 1 & 0 & 0 & 0 & 0 & 0 \\ (a_5)_j & 0 & (a_9)_j & (a_{11})_j & 0 & 0 & 0 & 0 & 0 \\ (b_5)_j & (b_9)_j & 0 & 0 & 0 & 0 & 0 & 0 & 0 \\ 0 & 0 & 0 & 0 & 0 & 0 & 0 & 0 & 0 \\ 0 & 0 & 0 & 0 & 0 & 0 & 0 & 0 & 0 \end{bmatrix}. \tag{41}$$